# All-electron spin–orbit configuration interaction study on the valence and low-lying Rydberg electronic states of GeH

**ARTICLE** *in* JOURNAL OF QUANTITATIVE SPECTROSCOPY AND RADIATIVE TRANSFER · MAY 2015

Impact Factor: 2.65 · DOI: 10.1016/j.jqsrt.2015.02.009



**6 AUTHORS**, INCLUDING:

Rui Li
Jilin University
**14** PUBLICATIONS **32** CITATIONS
SEE PROFILE

Xiaomei Zhang
Jilin University
**11** PUBLICATIONS **13** CITATIONS
SEE PROFILE

Mingxing Jin
Jilin University
**91** PUBLICATIONS **383** CITATIONS
SEE PROFILE

Bing Yan
Jilin University
**47** PUBLICATIONS **63** CITATIONS
SEE PROFILE

Journal of Quantitative Spectroscopy & Radiative Transfer 157 (2015) 42–53

Contents lists available at ScienceDirect

Journal of Quantitative Spectroscopy & Radiative Transfer

journal homepage: www.elsevier.com/locate/jqsrt

# All-electron spin–orbit configuration interaction study on the valence and low-lying Rydberg electronic states of GeH ☆

Rui Li [a,b], Zhen Zhai [c], Xiaomei Zhang [a], Mingxing Jin [a], Haifeng Xu [a,*], Bing Yan [a,*]

[a] Institute of Atomic and Molecular Physics, Jilin University, Changchun 130012, China
[b] Department of Physics, College of Science, Qiqihar University, Qiqihar 161006, China
[c] Laboratory of Optical Physics, Beijing National Laboratory for Condensed Matter Physics, Institute of Physics, Chinese Academy of Sciences, Beijing 100190, China

ARTICLE INFO

*Article history:*
Received 4 August 2014
Received in revised form
1 February 2015
Accepted 9 February 2015
Available online 18 February 2015

*Keywords:*
GeH
Spin–orbit coupling
Avoided crossing
Predissociation
Spectroscopic parameters

ABSTRACT

Germanium monohydride (GeH), an important radical for the growth of semiconductor germanium film, has received much attention. However, the electronic structure and spectroscopic properties of low-lying excited states of the radical have not been well understood, especially the coupling between different electronic states. In this work, eight Λ–S valence states and four low-lying Λ–S Rydberg states correlated to the four lowest dissociation limits of GeH are investigated by employing the multireference configuration interaction method. With the inclusion of spin–orbit coupling effect, there are 24 Ω states generated from 12 Λ–S states. On the basis of computed potential energy curves of the Λ–S and Ω states, the spectroscopic parameters of bound states are evaluated, which demonstrate that the first Rydberg state $3^2\Sigma^+$ located at 5.12 eV is exactly the $B^2\Sigma^+$ state tentatively assigned by experiment. With the help of the calculated spin–orbit matrix elements, the predissociation mechanism of $A^2\Delta$ state is investigated, which may interpret the fact that $v' > 2$ vibrational levels of $A^2\Delta$ state are difficult to be detected in experiment. Finally, the transition dipole moments and the radiative lifetimes of several vibrational levels of $A^2\Delta$ and $a^4\Sigma^-$ states are calculated.



## 1. Introduction

The spectroscopic properties of $GeH_n$ ($n$=1, 2, 3, 4) systems have continuously attracted attention over many years due to their applications in semiconductor industry. They play important roles in the growth of semiconductor films containing Ge atoms. It has been reported that one of the procedures is based on photodissociation of $GeH_4$ using a pulsed KrF (248 nm) excimer laser [1,2], resulting in the growth of semiconductor films via chemical vapor deposition. Existing experimental investigations indicated that the intermediate radicals GeH, $GeH_2$ and $GeH_3$ could affect the reaction kinetic from $GeH_4$ precursor to Ge thin films [2]. The thermochemical studies (such as dissociation properties, transition energies and vibrational frequencies) of $GeH_n$ can provide helpful information to understand photodissociaton process in the growth of Ge thin films [3]. In previous experimental work, the thermochemical data, dissociation properties, adiabatic ionization energies and electron affinities of $GeH_n$ ($n$=2–4) were measured by using mass spectroscopy [4–9], and the vibrational structure and electronic transition energies of $GeH_2$ [10–14] have also been well investigated. For the spectroscopic properties of GeH, there are also lots of experimental and theoretical studies.

☆ This paper is dedicated to the memory of Prof. Shoufu Pan

* Corresponding authors. Tel.: +86 431 85168817; fax: +86 431 85168816.
*E-mail addresses:* xuhf@jlu.edu.cn (H. Xu), yanbing@jlu.edu.cn (B. Yan).

http://dx.doi.org/10.1016/j.jqsrt.2015.02.009
0022-4073/

The spectra of GeH are well studied in experiment, especially for the low-lying electronic states. The visible and near-ultraviolet $a^4\Sigma^- - X^2\Pi$ and $A^2\Delta - X^2\Pi$ band spectra of the radical were first observed by Kleman and Werhagen [15,16]. The adiabatic transition energy $T_e$, rotational constant $B_e$, and equilibrium distances $R_e$ values of $a^4\Sigma^-$ are determined as 16,747 $cm^{-1}$, 6.7654 $cm^{-1}$, and 1.5834 Å, respectively. At the same time, Barrow et al. [17] observed another ultraviolet band system, which was tentatively assigned to $B^2\Sigma^+ - X^2\Pi$ transition. However, the spectroscopic properties of $B^2\Sigma^+$ were not discussed in detail. Klynning et al. [18] deduced the $T_e$ (25,454 $cm^{-1}$), $B_e$ (6.535 $cm^{-1}$), and $R_e$ (1.611 Å) values of $A^2\Delta$ state with rotational analysis of $A^2\Delta - X^2\Pi$ band. In the early 1990s, the infrared spectrum of the ground state $X^2\Pi$ of the radical was measured by different experimental methods, and the spectroscopic parameters of the $X^2\Pi$ state were obtained from the experimental spectrum [19–22].

Apart from these previous investigations that mainly focused on the spectroscopic parameters, several studies have been performed for the allowed transition dipole moments ($A^2\Delta - X^2\Pi$) and lifetimes of $A^2\Delta$ state. Erman et al. [23] measured the lifetimes of $A^2\Delta$ in the range of 75–85 ns and calculated the potential energy curves (PECs) of the $X^2\Pi$ and $A^2\Delta$ states. Based on the Frank–Condon factors (FCFs) and the transition dipole moments (TDMs) obtained from their study, the radiative lifetime of $A^2\Delta$ state was calculated to be 130 ns. Subsequently, Osmundsen et al. [24] also measured the radiative lifetime of the lowest vibrational level of the $A^2\Delta$ state, which is $12 \pm 2$ ns and independent of the vibrational quantum number. Later, Bauer et al. measured the radiative lifetime of $A^2\Delta$ state as $93 \pm 10$ ns [25] with laser-induced fluorescence (LIF) technique, and they explained that the discrepancy between the two experimental results [24,25] may arise from much higher partial pressures of $GeH_4$ ( > 1.5 Torr) used in experimental work [25], which can lead to a larger extrapolation range for the radiative lifetime of $A^2\Delta$ state.

Great theoretical effort on low-lying electronic states of the radical can also be found in previous works. Balasubramanian et al. [26] systematically studied the PECs for low-lying electronic states using the complete active space multiconfiguration self-consistent field (CASSCF) method followed by the first/second-order configuration interaction (FOCI/SOCI) calculation with a (4s4p6d/4s4p4d) Gaussian basis set in combination with 18-electrons ($1s^22s^22p^63s^23p^6$) relativistic effective core potential for Ge atom. The correlations of $3d^{10}$ electrons of Ge were not taken into account in their computations. The dipole moment ($\mu$), allowed TDMs, and the spectroscopic constants of several electronic states were obtained. They assigned the experimentally observed $B^2\Sigma^+$ state to $2^2\Sigma^+$ state, though the computed value of the adiabatic excited energy of $2^2\Sigma^+$ state is 0.32 eV lower than the experimental value of $B^2\Sigma^+$ state [17]. Subsequently, Bruna et al. [27] investigated the $X^2\Pi$ and $a^4\Sigma^-$ states of GeH with multireference configuration interaction (MRCI) approach, and reported the spectroscopic parameters of the two states. Recently, Song and Li et al. studied the electronic structures of $X^2\Pi$ [28,29] and $a^4\Sigma^-$ [29] states by means of high-level ab initio methods taking into account the spin–orbit (SO) coupling effect. Li et al. also used the complete basis set (CBS) extrapolation method to accurately predict the electronic structures and spectroscopic properties of $X^2\Pi$ and $a^4\Sigma^-$ states. The core-valence(CV) correlation of $3d^{10}$ electrons is included for the two electronic states. The influence of SO coupling effect on quartet–doublet energy differences and dissociation energies of the ground state were taken into consideration in their calculations.

As stated above, though a great deal of experimental and theoretical results on the electronic states of GeH are found, there still have some disagreements in previous works. For example, the assignment of the observed $B^2\Sigma^+$ state also needs more accurate ab initio calculations to reduce the large error (0.32 eV) between experimental value [17] and previous computational one [26]. In addition, as indicated in the study by Li et al. [29], the CV correlation effect of $3d^{10}$ electrons of Ge atom is important for the two lowest electronic states, so the improved ab initio results for higher excited states are expected to be obtained with inclusion of $3d^{10}$ CV correlations of Ge atom. In addition, the SO coupling effects, which play an important role in the excited-state structure and spectroscopy of radical containing heavy atom [30,31], are not systemically studied in the previous theoretical work.

The goal of present work is to obtain a detailed description on low-lying valence and Rydberg states as well as transition properties of excited states. We adopted ab initio MRCI method to calculate the low-lying electronic states of GeH. The PECs of eight Λ–S valence states, four low-lying Λ–S Rydberg states, and those of 24 Ω states generated from these Λ–S sates were obtained. The CV correlation and scalar relativistic effects were taken into account in our calculations. Based on the PECs, the spectroscopic parameters of electronic states were evaluated. Finally, the TDMs as well as lifetimes of $A^2\Delta$ and $a^4\Sigma^-$ states of the radical were obtained.

## 2. Methods and computational details

In the present work, the electronic structure calculations were performed with the Molpro2010 quantum chemical package [32]. The symmetry point group of GeH is $C_{\infty v}$. However, owing to the limitation of the Molpro program, all of the calculations were actually carried out in the $C_{2v}$ subgroup of $C_{\infty v}$ symmetry group. The heavy atom Ge has very obvious SOC effect. Hence, the calculated geometric structure of GeH is sensitive to the choice of basis sets, which will be discussed in detail in Section 3.1. The electronic states of GeH were computed with the state-averaged complete active space self-consistent field method (CASSCF) [33], followed by the internally contracted multireference configuration interaction method (MRCI) [34]. In the CASSCF calculations, the active space was composed of Ge 4s4p5s and H 1s shell, containing five electrons in six molecular orbitals. For the MRCI calculations, all configurations with a weight greater than 0.005 in the CI expansion were taken as reference, and the Davidson correction [35] (+Q) was also included to estimate the effect of higher electron excitation. The inner-shell $1s^22s^22p^6$ $3s^23p^6$ electrons of Ge atom were

kept frozen. However, the $3d^{10}$ electrons of Ge atom were correlated to account for the CV correction. That is to say, 15 electrons in total in GeH (excluding $1s^22s^22p^63s^23p^6$ electrons of Ge) were correlated in the MRCI calculations.

In all calculations, the scalar relative effect was obtained from the third-order Douglas–Kroll [36] and Hess [37] one-electron integrals. The SO coupling effect was taken into account via calculating full Breit–Pauli Hamiltonian ($H_{BP}$) with the state-interacting method, and the spin–orbit part of the full $H_{BP}$ is written as

$$\hat{H}^{SO}=\frac{e^2}{2m_e^2c^2}\sum_i\left[\sum_K\frac{Z_K}{r_{iK}^3}\left[\vec{r}_{iK}\times\vec{p}_i\right]\cdot\vec{s}_i-\sum_{j\neq i}\frac{1}{r_{ij}^3}\left[\vec{r}_{ij}\times\vec{p}_i\right]\cdot\left[\vec{s}_i+2\vec{s}_j\right]\right], \quad (1)$$

where $e$ is the charge of electron, $m_e$ is the mass of the electron, $c$ is the speed of light, $\vec{r}_{iK}=\vec{r}_i-\vec{R}_K$ is the $i$-th position vector with respect to the nucleus K, $Z_k$ is the electronic charge of nucleus K, $\vec{s}_i$ is the spin operator of electron $i$, and $r_{ij}$ describes the distance between electrons $i$ and $j$. In the SO coupling calculations, the SO eigenvalues were obtained by diagonalizing $\hat{H}^{el}+\hat{H}^{SO}$ in the basis eigenfunctions of $\hat{H}^{el}$. In addition, the $\hat{H}^{el}$ matrix elements were obtained from MRCI+Q computations, and the $\hat{H}^{so}$ matrix elements were evaluated with MRCI wave functions.

On the basis of calculated PECs of the Λ–S and Ω electronic states, vibrational energy levels, vibrational wave functions, and spectroscopic constants were determined by numerical solutions of the nuclear Schrödinger equations, employing LEVEL procedure designed by LeRoy [38]. The radiative lifetime of vibrational state was calculated by summing the Einstein coefficients for each of downward transitions and inverting them.

## 3. Results and discussion

### 3.1. Choice of basis set and core-valence correction of $3d^{10}$ electrons of Ge

The SO splittings of energy levels of heavy atom Ge are influenced by the selection of basis set and the number of correlated electrons in the MRCI calculations. To calibrate the influence of basis set and CV correlation on computations, different basis set species, including aug-cc-pVnZ-DK (AVnZ-DK)[39,40], aug-cc-pCVnZ-DK (ACVnZ-DK) [40,41], and aug-cc-pwCVnZ-DK (AWCVnZ-DK) [$n=T(3),Q(4),5$] [39–41] were firstly used to compute the $^3$P energy levels of Ge atom. Our calculated $^3$P energy levels of Ge atom and the corresponding experimental results are listed in Table 1. It can be seen from Table 1 that the SO splitting energies of $^3P_0$–$^3P_1$ and $^3P_0$–$^3P_2$ are distinctly dependent on the choice of basis set and CV correction of $3d^{10}$ electrons of Ge atom. With $n$ increasing from 3 to 5 for AVnZ-DK, ACVnZ-DK, and AWCVnZ-DK basis sets, the calculated SO splitting energies of $^3P_0$–$^3P_1$ and $^3P_0$–$^3P_2$ gradually approach the experimental values of 557.13 and 1409.96 $cm^{-1}$ [42], respectively. However, with excluding the CV correction of $3d^{10}$ electrons of Ge, the calculated splitting energies of $^3P_0$–$^3P_1$ and $^3P_0$–$^3P_2$ are still underestimated by 59.05 and 144.76 $cm^{-1}$, as compared to the previously measured values [42]. When the CV correction of $3d^{10}$ electrons of Ge is taken into consideration, the best calculated splitting energies of $^3P_0$–$^3P_1$ and $^3P_0$–$^3P_2$ (using AWCV5Z-DK basis set) are 533.45 $cm^{-1}$ and 1340.90 $cm^{-1}$, respectively, which differ by only 23.68 and 69.06 $cm^{-1}$ from the measured values of 557.13 and 1409.96 $cm^{-1}$ [42]. Thus, in the subsequent calculations, we employ aug-cc-pwCV5Z-DK [39–41] and aug-cc-pV5Z-DK [43] to describe Ge and H atoms, respectively.

### 3.2. PECs of the Λ–S states of GeH

The eight Λ–S valence states and four low-lying Λ–S Rydberg states correlated to the four lowest dissociation limits ($Ge(^3P_g)+H(^2S_g)$, $Ge(^1D_g)+H(^2S_g)$, $Ge(^1S_g)+H(^2S_g)$, and $Ge(^3P_u)+H(^2S_g)$ ) of GeH, which are computed by the MRCI+Q approach. The PECs of the 12 Λ–S states are depicted in Fig. 1. It can be found that $X^2\Pi$, $a^4\Sigma^-$, $A^2\Delta$, $2^2\Sigma^+$, $2^2\Sigma^+$, $2^4\Pi$, and $3^2\Pi$ states are typical bound states, and the other five states are repulsive states. The spectroscopic parameters ($T_e$, $\omega_e$, $\omega_e x_e$, $B_e$, $\alpha_e$, and $R_e$) of the bound states are listed in Table 2. The spectroscopic parameters obtained from previous studies are also given in Table 2 for

**Table 1**
Spin–orbit splitting between the $^3P_0$–$^3P_1$ and $^3P_0$–$^3P_2$ terms in the Ge atom.

| Method | Spin–orbit splitting | | Method | Spin–orbit splitting | |
|---|---|---|---|---|---|
| MRCI+Q (4s4p)[a] | $^3P_0$–$^3P_1$ | $^3P_0$–$^3P_2$ | MRCI+Q (3d4s4p)[b] | $^3P_0$–$^3P_1$ | $^3P_0$–$^3P_2$ |
| AVTZ-DK | 490.27 | 1251.84 | AVTZ-DK | 495.42 | 1262.91 |
| AVQZ-DK | 494.49 | 1260.22 | AVQZ-DK | 500.61 | 1271.99 |
| AV5Z-DK | 497.51 | 1262.20 | AV5Z-DK | 523.02 | 1317.70 |
| ACVTZ-DK | 491.65 | 1255.39 | ACVTZ-DK | 521.15 | 1319.49 |
| ACVQZ-DK | 496.77 | 1263.35 | ACVQZ-DK | 530.05 | 1334.77 |
| ACV5Z-DK | 497.94 | 1264.96 | ACV5Z-DK | 532.63 | 1339.14 |
| AWCVTZ-DK | 493.02 | 1258.20 | AWCVTZ-DK | 526.02 | 1328.97 |
| AWCVQZ-DK | 496.93 | 1263.67 | AWCVQZ-DK | 532.06 | 1338.89 |
| AWCV5Z-DK | 498.08 | 1265.20 | AWCV5Z-DK | 533.45 | 1340.90 |
| Expt.[c] | 557.13 | 1409.96 | | 557.13 | 1409.96 |

[a] MRCI+Q(4s4p) denotes that $4s^24p^2$ electrons of Ge atom were correlated in the MRCI calculations.
[b] MRCI+Q(4s4p3d) denotes that $3d^{10}4s^24p^2$ electrons of Ge atom were correlated in the MRCI calculations.
[c] Ref. [42].

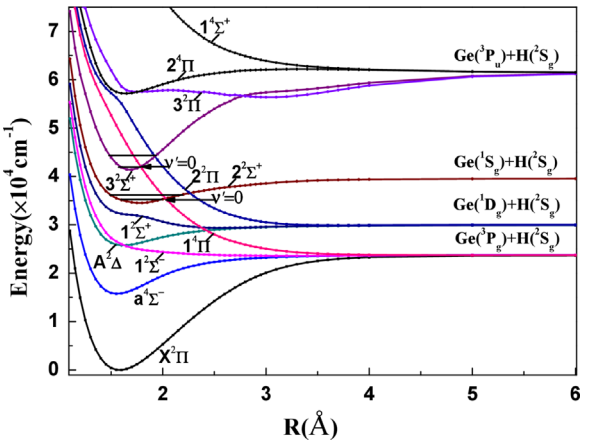


**Fig. 1.** Calculated MRCI+Q potential energy curves of eight Λ–S valence states and four low-lying Rydberg states, excluding the spin–orbit coupling interaction. These states are given in energy relative to the minimum energy point of $X^2\Pi$ state.

comparison. The spectroscopic parameters of bound states were obtained in two different ways, that is, including and excluding the CV correction of $3d^{10}$ electrons of Ge atom.

The ground state of GeH is $X^2\Pi$ state with $8\sigma^2 9\sigma^2 4\pi^1$ electronic configuration (the electronic configuration of Λ–S states are provided as Supplement material in Table S1). For the ground state, when the CV effect is excluded, the calculated values of $\omega_e$, $\omega_e x_e$, $B_e$, and $R_e$ are accurate with the deviations of 146.49 $cm^{-1}$, 0.5091 $cm^{-1}$, 0.1030 $cm^{-1}$, and 0.0141 Å relative to the latest experimental results, respectively [22]. In addition, when the CV correction is included, the spectroscopic constants $\omega_e$, $\omega_e x_e$, $B_e$, and $R_e$ are improved by 132 $cm^{-1}$ (6%), 0.22 $cm^{-1}$ (0.7%), 0.14 $cm^{-1}$ (2%), and 0.019 Å (1%), respectively. The previous experimental values of $\omega_e$ have a discrepancy as large as ~67 $cm^{-1}$ (1833.77 [44] vs. 1900.38 [22]). While the previous computational works present consistent results in the range of 1884–1930 $cm^{-1}$ at different levels of theory [26–29]. Our best computed $\omega_e$ value (1914.93 $cm^{-1}$) is close to the previous theoretical value [28] at multiconfiguration quasidegenerate second-order perturbation theory (MCQDPT2) level within 2 $cm^{-1}$, and slightly differs from the latest experimental value [22] and recent computational value [29] at CCSD(T)/cc-pV5Z level with errors of ± 15 $cm^{-1}$. Our computation results also indicate that the CV correction leads to a significant improvement (132 $cm^{-1}$ or 6%) on the $\omega_e$ value. Whether the CV correction is concerned or not, our computational results of $\omega_e x_e$ and $B_e$ are consistent with the theoretical results by Song et al. [28], and accord with the measurement values by Towle et al. [22]. Compared with experimental results, our best computed $R_e$ is only ~0.005 Å underestimated, and agrees excellently with recent extrapolated result at CCSD(T)/CBS level [29]. Compared with most previous computational works [26–28], our results of $D_e$ are improved by 0.06–0.2 eV, and especially by 0.02 eV by including the CV effect. In addition, our computed $D_e$ value (2.94 eV) falls exactly into the error bar of the experimental value (3.1 ± 0.2 eV), and agrees excellently with recent couple-cluster result [29]. Our best calculated $\alpha_e$ is 0.1925 $cm^{-1}$, which agrees well with a previous experimental result of 0.191 $cm^{-1}$ [44].

The first excited sate $a^4\Sigma^-$ arises from the electronic configuration $8\sigma^2 9\sigma^1 4\pi^2$. According to the present computational results, the CV effect leads to corrections of 16 $cm^{-1}$ (0.1%), 143 $cm^{-1}$ (7%), 15 $cm^{-1}$ (13%), and 0.016 Å (1%) on $T_e$, $\omega_e$, $\omega_e x_e$, and $R_e$ values of $a^4\Sigma^-$ state, respectively. Our computed $T_e$ including the CV correction differs only ~110 $cm^{-1}$ from the recent high-level theoretical value with CCSD(T) method [29], and also reasonably agrees with experimental values [15]. With the inclusion of CV correction, the $\omega_e$ and $R_e$ values are computed to be 1800.74 $cm^{-1}$ and 1.5562 Å, respectively, which are in good accordance with recent high-level theoretical values of 1844 $cm^{-1}$ and 1.559 Å [29]. Our calculated value of $\omega_e$ is also in good agreement with the theoretical values of 1780 $cm^{-1}$ [27]. However, the deviation of $R_e$ for the $a^4\Sigma^-$ state between experiment [15] and the above two high-level ab initio calculations (this work and Ref. [29]) is as large as ~0.02 Å, which suggests that experimental effort should be made to decrease the gap between experiment and ab initio calculations. Our computed values show consistence in dissociation energy. The CV correlations contribute a correction of −0.01 eV to $D_e$ of the $a^4\Sigma^-$ state, which agrees with a previous theoretical value of 1.1 eV [27].

The second excited state $A^2\Delta$ originates from the electronic configuration $8\sigma^2 9\sigma^1 4\pi^2$, which is the same as that of the first excited sate $a^4\Sigma^-$. Without the CV correction, the calculated $T_e$, $B_e$, and $R_e$ values only differ from the corresponding experimental values by 775 $cm^{-1}$, 0.0355 $cm^{-1}$, and 0.0082 Å, respectively [18]. Moreover, with inclusion of the CV correction, the spectroscopic constants $T_e$, $\omega_e$, $\omega_e x_e$, $B_e$, and $R_e$ are corrected by 1095 $cm^{-1}$ (4%),132 $cm^{-1}$ (9%), 9 $cm^{-1}$ (8%), 0.03 $cm^{-1}$ (0.5%), and 0.002 Å (0.1%), respectively, and the differences between the experimental values [18,44] and our calculated ones of $T_e$, $B_e$, $\alpha_e$ and $R_e$ are only 320 $cm^{-1}$, 0.0007 $cm^{-1}$, 0.018 $cm^{-1}$, and 0.006 Å, respectively. The $D_e$ value in our work is predicted to be as twice as that in previous theoretical work [26]. Thus, more vibrational levels are expected to exist in the potential well of the $A^2\Delta$ state.

As shown in previous investigations of isoelectronic CH and SiH radicals [45,46], the three lowest $^2\Sigma^+$ states may interact among themselves. Thus we list the electronic configurations of the three $^2\Sigma^+$ states at three different bond lengths ($R$=1.4 Å, 1.7 Å, and 2.0 Å) in Table S1. It can be seen from Table S1 that the dominant electronic configurations of $1^2\Sigma^+$, $2^2\Sigma^+$, and $3^2\Sigma^+$ states are $8\sigma^2 9\sigma^1 4\pi^2$, $8\sigma^2 9\sigma^2 10\sigma^1$, and $8\sigma^2 9\sigma^2 11\sigma^1$ in the Franck–Condon region, respectively. In addition, at the bond length near $R_e$ ($R$=1.4 Å and 1.7 Å), the electronic configurations of the three $^2\Sigma^+$ states mix with each other. Our computations indicate that valence and Rydberg excitations are mixed in $2^2\Sigma^+$ and $3^2\Sigma^+$ electronic states, the electronic configurations of these two states are mainly described by one-electron excitations to 1sσ orbital of H and 5sσ Rydberg orbital of Ge from 4pπ orbital of Ge. In previous experiment, the band system in $B^2\Sigma^+$–$X^2\Pi$ transition was observed [17], and the transition energies $T_e$ and $T_{00}$ of observed $B^2\Sigma^+$ state were determined as 41,074 [17] and 39,385.6 $cm^{-1}$ [24], respectively. Two

**Table 2**
Computed and experimental spectroscopic constants of bound Λ–S states of GeH.

| State | Method | $T_e$ (cm$^{-1}$) | $\omega_e$ (cm$^{-1}$) | $\omega_e x_e$ (cm$^{-1}$) | $B_e$ (cm$^{-1}$) | $\alpha_e$ (cm$^{-1}$) | $R_e$ (Å) | $D_e$ (eV) | DM (a.u.) |
|---|---|---|---|---|---|---|---|---|---|
| $X^2\Pi$ | MRCI+Q[a] | 0 | 1914.93 | 33.2176 | 6.7688 | 0.1925 | 1.5823 | 2.94 | 0.026 (0.066 D) |
| | MRCI+Q[b] | 0 | 2046.87 | 32.9933 | 6.6271 | | 1.6013 | 2.96 | |
| | Expt.[c] | 0 | 1833.77 | 37 | 6.7259 | 0.191(6) | 1.5880 | 3.1(2) | |
| | Expt.[d] | 0 | 1900.3820 | 33.5024 | 6.7300 559 | | 1.58724 | | |
| | Calc.[e] | 0 | 1899 | | | | 1.594 | 2.74 | |
| | Calc.[f] | 0 | 1884 | 45 | 6.504 | | 1.60816 | 2.86 | |
| | Calc.[g] | 0 | 1913.72 | 31.356 | 6.603 | | 1.6027 | 2.877 | |
| | Calc.[h] | 0 | 1930 | | | | 1.584 | 2.95 | 0.083 D |
| | Calc.[i] | | | | | | | | 0.097 D |
| $a^4\Sigma^-$ | MRCI+Q[a] | 15,770 | 1800.74 | 101.5430 | 7.0172 | 0.3947 | 1.5562 | 1.00 | 0.001 (0.025 D) |
| | MRCI+Q[b] | 15,754 | 1943.62 | 116.1794 | 6.8519 | | 1.5728 | 1.01 | |
| | Expt.[j] | 16,747 | | | 6.7654 | | 1.5834 | | |
| | Calc.[e] | 13,914 | 1637 | | | | 1.6 | 0.74 | |
| | Calc.[f] | 14,195 | 1780 | 62 | 6.806 | | 1.58330 | 1.10 | |
| | Calc.[h] | 15,881 | 1844 | | | | 1.559 | | 0.172D |
| $A^2\Delta$ | MRCI+Q[a] | 25,774 | 1306.36 | 104.3838 | 6.5343 | 0.6370 | 1.6170 | 0.52 | 0.140 |
| | MRCI+Q[b] | 24,679 | 1438.73 | 113.2515 | 6.4995 | | 1.6192 | 0.58 | |
| | Expt.[c] | 25,454 | 1185.15 | 127 | 6.535 | 0.619(6) | 1.611 | | |
| | Expt.[k] | 25,454 | | | 6.535 | | 1.611 | | |
| | Calc.[e] | 26,663 | 1302 | | | | 1.66 | 0.26 | |
| $2^2\Sigma^+$ | MRCI+Q[a] | 34,538 | 1109.54 | 61.7387 | 5.4687 | 0.3464 | 1.7819 | 0.62 | −0.157 |
| | MRCI+Q[b] | 32,459 | 1292.22 | 69.4002 | 5.3890 | | 1.7792 | 0.76 | |
| | Calc.[e] | 38,528 | 1362 | | | | 1.83 | 0.56 | |
| $B^2\Sigma^+$ ($3^2\Sigma^+$) | MRCI+Q[a] | 41,264 | 2260.72 | 82.8077 | 6.0328 | 0.1247 | 1.6786 | 2.38 | −0.738 |
| | MRCI+Q[b] | 37,672 | 2318.18 | 52.2197 | 6.4765 | | 1.6205 | 2.76 | |
| | Expt.[l] | 41,074 | | | | | | | |
| | Expt.[m] | 39,385.6 | | | | | | | |
| | Calc.[e] | 46,267 | 2107 | | | | 1.67 | | |
| $2^4\Pi$ | MRCI+Q[a] | 57,164 | 1530.71 | 111.4764 | 6.3211 | 0.4757 | 1.6389 | 0.54 | 0.949 |
| | MRCI+Q[b] | 56,036 | 1656.04 | 116.8629 | 6.4139 | | 1.6271 | 0.63 | |
| $3^2\Pi$ | MRCI+Q[a] | 53,365 | 632.11 | 7.2502 | 1.7074 | −0.0039 | 3.1525 | 0.95 | −2.289 |
| | MRCI+Q[b] | 48,712 | 572.18 | 3.9050 | 1.5514 | | 3.3046 | 1.35 | |

[a] Computed values using aug-cc-pwCV5Z-DK (Ge) and aug-cc-pV5Z-DK (H) basis sets with inclusion of core-valence effect of $3d^{10}$ electrons of Ge in this work.
[b] Computed values using aug-cc-pwCV5Z-DK (Ge) and aug-cc-pV5Z-DK (H) basis sets with exclusion of core-valence effect of $3d^{10}$ electrons of Ge in this work.
[c] Ref. [44].
[d] Ref. [22].
[e] Ref. [26].
[f] Ref. [27].
[g] Ref. [28].
[h] Ref. [29].
[i] Ref. [49].
[j] Ref. [15].
[k] Ref. [18].
[l] Ref. [17].
[m] $T_{00}$ value in Ref. [24].

bound states, $2^2\Sigma^+$ and $3^2\Sigma^+$, with $T_e$ values of 38,528 and 46,267 cm$^{-1}$, respectively, were found in previous theoretical work [26]; and the $2^2\Sigma^+$ state was assigned to the experimentally observed $B^2\Sigma^+$ state in previous theoretical work [26], despite a deviation of 2546 cm$^{-1}$ (0.32 eV) exists between the computation and experimental results. Our computations demonstrate that the CV correlation significantly contributes (~2000 cm$^{-1}$ and ~3500 cm$^{-1}$) to the transition energies of $2^2\Sigma^+$ and $3^2\Sigma^+$ states, respectively. The most accurate value we obtained for $T_e$ (41,264 cm$^{-1}$) of the $3^2\Sigma^+$ state agrees very well with the experimentally determined value [17] within 200 cm$^{-1}$, because the present $T_e$ (34,538 cm$^{-1}$) of the $2^2\Sigma^+$ state at the same level of theory is 6536 cm$^{-1}$ smaller than that of the $B^2\Sigma^+$ state, we suggest that the experimentally observed $B^2\Sigma^+$ state should be assigned to the $3^2\Sigma^+$ state instead of the $2^2\Sigma^+$ state assigned in previous theoretical work [26]. Our calculated $T_{00}$ of the $B^2\Sigma^+$ state is 40,491 cm$^{-1}$, which also agrees well with the previously observed value of 39,385.6 cm$^{-1}$ [24]. The spectroscopic constants of these two states are listed in Table 2 for further experimental comparisons.

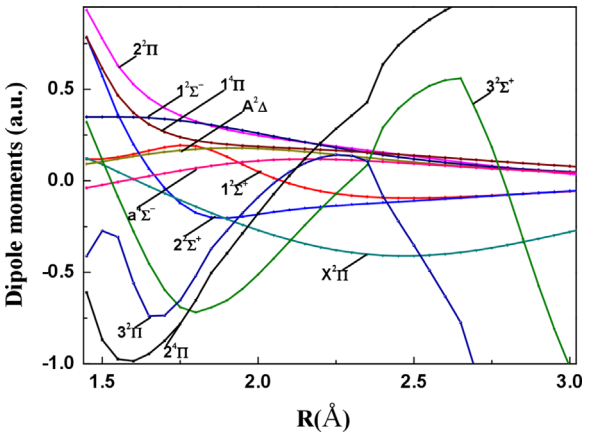


**Fig. 2.** Evolution of dipole moments for low-lying Λ–S states along the internuclear distance.

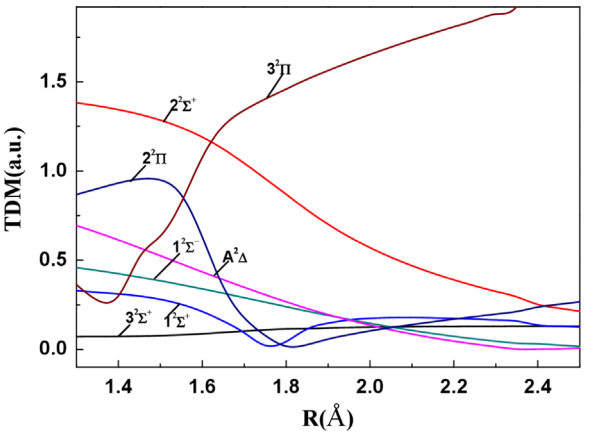


**Fig. 3.** The calculated electronic transition dipole moments for low-lying Λ–S states as a function of internuclear distance.

Apart from the $3^2\Sigma^+$ state, other two bound states $3^2\Pi$ and $2^4\Pi$ correlated to the Ge(4p5s,$^3P_u$)+H(1s,$^2S_g$) limit are characterized by our computations, as listed in Table 2. These two electronic states are mainly described by $8\sigma^2 9\sigma^1 10\sigma^1 4\pi^1$ and $8\sigma^2 9\sigma^1 11\sigma^1 4\pi^1$. The spectroscopic constants of the two states have been neither experimentally obtained nor theoretically evaluated in the previous works, and the present theoretical result can provide support for future spectroscopic study of the two states.

In previous studies, the dipole moment for $X^2\Pi$ has been comprehensively investigated. The previously available theoretical dipole moment for $X^2\Pi$ is distributed in the region from 0.053 to 0.11 Debye (D) [26,47–49]. However, the only experimental dipole moment for $X^2\Pi$ obtained by Brown et al. [50] is $1.24 \pm 0.10$ D, which differs from the known theoretical results in the order of magnitude. Due to the large overestimation of experimental results relative to theoretical results, Ashworth and Brown reconsidered the formalism [51] used to analyze experimental results. Their studies indicated that the previous procedure has some questions, because the electronic transition moments were omitted in the formalism used to extract dipole moment. However, owing to the absence of such information of GeH, they were unable to give a revised dipole moment of the radical. Chapman et al. [49] and Li et al. [29] calculated the dipole moment of the radical to be 0.097 and 0.083 D at relativistic CI formalism and CCSD(T)/cc-pV5Z level, respectively. Our calculated dipole moment curves of low-lying Λ–S states at the MRCI+Q/ aug-cc-pwCV5Z-DK level are plotted in Fig. 2. The dipole moment for $X^2\Pi$ is 0.066 D (1 a.u.=2.54 D) at the equilibrium distance. Our calculated value of the dipole moment for $X^2\Pi$ conforms well to the recent couple-cluster computation [29]. The calculated dipole moments of low-lying excited states at $R_e$ are given in Table 2. The dipole moment for $a^4\Sigma^-$ is 0.025 D, which is smaller than previous theoretical result 0.172 D [29]. As shown in Fig. 2, all the dipole moments tend to be zero as $R \to \infty$, demonstrating that dissociation products are neutral atoms.

The electronic TDMs of doublet states were calculated at the MRCI level. The TDMs of all doublet states along with the bond length are plotted in Fig. 3. As shown in Fig. 3, at the bond length of $R=3.0$ a.u., the TDMs of $A^2\Delta$ is 0.43 a.u., which is consistent with previous theoretical results of 0.31 a.u. [49] and 0.5537 a.u. [23]. On the basis of calculated TDMs and PECs of excited states, we calculate the oscillator strength (*f*-value) of all doublet states ($A^2\Delta$, $1^2\Sigma^-$, $1^2\Sigma^+$, $2^2\Sigma^+$, $2^2\Pi$, $3^2\Sigma^+$, and $3^2\Pi$), which are listed in Table 3. The vertical excitation energies of these doublet states are also given in Table 3. It can be seen from Table 3 that strong absorption could occur at 35,245 $cm^{-1}$ (284 nm) and 57,386 $cm^{-1}$ (174 nm) corresponding to $2^2\Sigma^+$ and $3^2\Pi$ transitions, respectively. The *f*-values of $A^2\Delta$, $2^2\Pi$, and $3^2\Sigma^+$ states are in $10^{-2}$ order of magnitude, and the transitions to $1^2\Sigma^-$ and $1^2\Sigma^+$ states are weak, the *f*-values of which are one order smaller.

**Table 3**
The oscillator strength *f*-values and vertical excitation energies of doublet states.

| State | Oscillator strength *f*-values (a.u.) at $R_e$ | Vertical excitation energies ($cm^{-1}$) |
|---|---|---|
| $A^2\Delta$ | 0.01612 | 25,651 |
| $1^2\Sigma^-$ | 0.00979 | 26,389 |
| $1^2\Sigma^+$ | 0.00512 | 32,293 |
| $2^2\Sigma^+$ | 0.15693 | 35,245 |
| $2^2\Pi$ | 0.09016 | 55,664 |
| $3^2\Sigma^+$ | 0.09254 | 42,134 |
| $3^2\Pi$ | 0.17345 | 57,386 |

### 3.3. PECs of Ω states and analysis of avoided crossing phenomenon in GeH

As a kind of relativistic effect, the SO coupling effect leads to the splitting of multiplet electronic states and recombination of Λ–S states with the same Ω symmetry component. When the SO coupling effect is taken into consideration, the lowest dissociation limit of Ge($^3P_g$)+H($^2S_g$) splits into three asymptotes, namely, Ge($^3P_{0g}$)+H($^2S_{1/2g}$), Ge($^3P_{1g}$)+H($^2S_{1/2g}$), and Ge($^3P_{2g}$)+H($^2S_{1/2g}$); the second and third dissociation limits (Ge($^1D_{2g}$)+H($^2S_{1/2g}$) and Ge($^1S_{0g}$)+H($^2S_{1/2g}$)) are associated with singlet states of Ge and H atoms. Hence, the SO splitting does not exist in the

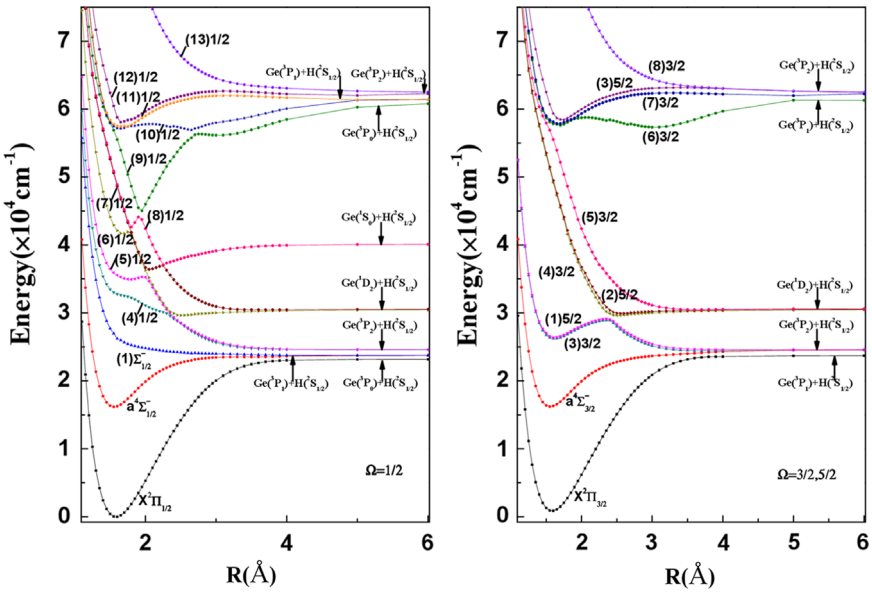


**Fig. 4.** Calculated spin–orbit configuration interaction potential energy curves of the low-lying electronic states for $\Omega=1/2$ (left) and $\Omega=3/2$, 5/2 (right) states.

**Table 4**
Dissociation relationship of low-lying Ω states of GeH.

| Atomic state (Ge+H) | Ω state | Energy($cm^{-1}$) | |
|---|---|---|---|
| | | This work | Expt.[a] |
| $^3P_{0g}+^2S_{1/2g}$ | 1/2 | 0 | 0 |
| $^3P_{1g}+^2S_{1/2g}$ | 1/2,1/2,3/2 | 533.45 | 557.13 |
| $^3P_{2g}+^2S_{1/2g}$ | 1/2,1/2,3/2,3/2,5/2 | 1340.90 | 1409.96 |
| $^1D_{2g}+^2S_{1/2g}$ | 1/2,1/2,3/2,3/2,5/2 | 7208.37 | 7125.30 |
| $^1S_{0g}+^2S_{1/2g}$ | 1/2 | 16,447.93 | 16,367.33 |
| $^3P_{0u}+^2S_{1/2g}$ | 1/2 | 37,917.22 | 37,451.69 |
| $^3P_{1u}+^2S_{1/2g}$ | 1/2,1/2,3/2 | 38,399.15 | 37,702.31 |
| $^3P_{2u}+^2S_{1/2g}$ | 1/2,1/2,3/2,3/2,5/2 | 39,408.76 | 39,117.90 |

[a] Ref. [42].

two dissociation limits. The fourth dissociation limit also splits into three asymptotes, namely, $Ge(^3P_{0u})+H(^2S_{1/2g})$, $Ge(^3P_{1u})+H(^2S_{1/2g})$, and $Ge(^3P_{2u})+H(^2S_{1/2g})$.

There are 24 $\Omega$ states associated with the eight lowest dissociation limits of the GeH molecule. Their PECs are given in Fig. 4, including 13 $\Omega=1/2$, eight $\Omega=3/2$, and three $\Omega=5/2$. The dissociation limits for the Ω states and the corresponding energy separations are illustrated in Table 4. The calculated energy separations of these dissociation limits relative to the lowest dissociation limit are 533.45, 1340.90, 7208.37, 16,447.93, 37,917.22, 38,399.15, and 39,408.76 $cm^{-1}$, respectively, which are in excellent agreement with experimental results of 557.13, 1409.96, 7125.30, 16,367.33, 37,451.69, 37,702.31, and 39,117.90 $cm^{-1}$ [42].

On the basis of the calculated Ω-state PECs, the spectroscopic parameters of the GeH molecule were evaluated with numerical method and listed in Table 5. The dominant Λ–S compositions of low-lying Ω states at different internuclear distances are given in Table 6. When consider the second-order contributions (SO coupling between
$X^2\Pi$ and excited states of the four lowest dissociation limits), the calculated SO splitting of $X^2\Pi$ is 869 $cm^{-1}$, which is consistent with the latest experimental result of 892.628 $cm^{-1}$ [22]. Our calculated value also agrees reasonably with previous theoretical values of 755.760 [28], 869 $cm^{-1}$ [26], and 913.14 $cm^{-1}$ [52]. The SO matrix elements including some selected states ($X^2\Pi$, $a^4\Sigma^-$, $A^2\Delta$, $1^2\Sigma^+$, $2^2\Sigma^+$ and $3^2\Sigma^+$) are listed in Table S2 of supplement materials. As shown in Table S2, at the Franck–Condon region, the SO matrix elements between $X^2\Pi$ and the three lowest $^2\Sigma^+$ states are on the order of 100 $cm^{-1}$, and the strong interactions of these states can affect the dipole moments of $X^2\Pi$ state and the TDMs of the three lowest $^2\Sigma^+$ states. At the equilibrium distance, the dipole moment of $X^2\Pi_{1/2}$ is 0.055 D, which are 0.011 D smaller than the dipole moment of $X^2\Pi$. Near the equilibrium, the SO matrix elements of $a^4\Sigma^- – X^2\Pi$ is about 110 $cm^{-1}$, which can cause the forbidden transition $a^4\Sigma^- – X^2\Pi$ as illuminated in Ref. [53] and the change of dipole moment of the $a^4\Sigma^-$ state. At the equilibrium distance, the dipole moment of $a^4\Sigma-$ 1/2 is 0.099 D, which is corrected by 0.074 D as compared with that of the $a^4\Sigma^-$ state. In addition, the SO matrix elements of $A^2\Delta–X^2\Pi$, $A^2\Delta–2^2\Pi$, $A^2\Delta–3^2\Pi$, $A^2\Delta–1^4\Pi$, and $A^2\Delta–2^4\Pi$ are all on the order of 100 $cm^{-1}$, which can cause obvious SO splitting of the $A^2\Delta$ state as illustrated in Ref. [54].

As shown in Table 6, the dominant Λ–S compositions of $X^2\Pi_{1/2}$ and $X^2\Pi_{3/2}$ states are almost pure $^2\Pi$ state near the equilibrium internuclear distance. Hence, the spectroscopic parameters ($\omega_e$, $\omega_e x_e$, $B_e$, $\alpha_e$, and $R_e$) for $X^2\Pi_{1/2}$ and $X^2\Pi_{3/2}$ states are almost the same as those of the $X^2\Pi$ state. The $D_e$ of $X^2\Pi_{1/2}$ is calculated to be 2.87 eV, which is well consistent with the latest theoretical values of 2.88

**Table 5**
Computed and experimental spectroscopic constants of low-lying Ω states of GeH.

| State | Method | $T_e$ ($cm^{-1}$) | $\omega_e$ ($cm^{-1}$) | $\omega_e x_e$ ($cm^{-1}$) | $B_e$ ($cm^{-1}$) | $\alpha_e$ ($cm^{-1}$) | $D_e$ (eV) | $R_e$ (Å) |
|---|---|---|---|---|---|---|---|---|
| $X^2\Pi_{1/2}$ | MRCI+Q+SOC[a] | 0 | 1913.28 | 33.2201 | 6.7684 | 0.1932 | 2.87 | 1.5824 |
| | Expt.[b] | 0 | 1900.3820 | 33.5024 | 6.7300 | | | 1.58724 |
| | Calc.[c] | 0 | 1806 | | | | 2.34 | 1.62 |
| | Calc.[d] | 0 | 1900.556 | 31.372 | 6.598 | | 2.880 | 1.6033 |
| | Calc.[e] | 0 | | | | | 2.89 | |
| $X^2\Pi_{3/2}$ | MRCI+Q+SOC[a] | 869 | 1916.85 | 33.4005 | 6.7701 | 0.1921 | 2.83 | 1.5821 |
| | Expt.[b] | 892.628 | | | | | | |
| | Calc.[c] | 869 | 1810 | | | | 2.30 | 1.62 |
| | Calc.[d] | 755.760 | 1905.047 | 31.595 | 6.606 | | 2.877 | 1.6023 |
| $a^4\Sigma^-_{1/2}$ | MRCI+Q+SOC[a] | 16,189 | 1873.02 | 114.4706 | 7.0150 | 0.3257 | 0.94 | 1.5565 |
| $a^4\Sigma^-_{3/2}$ | MRCI+Q+SOC[a] | 16,227 | 1660.96 | 83.4046 | 7.0162 | 0.3253 | 1.03 | 1.5563 |
| (3)3/2 ($A^2\Delta_{3/2}$) | MRCI+Q+SOC[a] | 26,221 | 1401.69 | 119.7869 | 6.5404 | 0.3864 | 0.70 | 1.6175 |
| (1)5/2 ($A^2\Delta_{3/2}$) | MRCI+Q+SOC[a] | 26,415 | 1449.49 | 142.1317 | 6.5257 | 0.4891 | 0.85 | 1.6108 |
| (4)3/2 | MRCI+Q+SOC[a] | 29,645 | 448.51 | 74.4988 | 2.6721 | 0.6253 | 0.10 | 2.4837 |
| (2)5/2 | MRCI+Q+SOC[a] | 29,943 | 354.48 | 66.2360 | 2.6318 | 0.7927 | 0.08 | 2.5592 |
| (6)3/2 | MRCI+Q+SOC[a] Inner well | 57,616 | | | | | | 1.7029 |
| | MRCI+Q+SOC[a] Outer well | 57,332 | 418.62 | 9.8403 | 1.8130 | −0.1351 | 0.55 | 3.0331 |
| (7)3/2 | MRCI+Q+SOC[a] | 57,845 | 1562.07 | 265.9070 | 0.6075 | 0.4693 | 0.60 | 1.6751 |
| (3)5/2 | MRCI+Q+SOC[a] | 58,433 | 1660.12 | 144.2060 | 5.7814 | 0.5632 | 0.59 | 1.7346 |
| (5)1/2 | MRCI+Q+SOC[a] | 34,950 | | | | | | 1.7876 |
| (6)1/2 | MRCI+Q+SOC[a] | 41,676 | | | | | | 1.6803 |

[a] The calculation was employed using aug-cc-pwCV5Z-DK (Ge) and aug-cc-pV5Z-DK (H) basis sets.
[b] Ref. [22].
[c] Ref. [26].
[d] Ref. [28].
[e] Ref. [29].

[28] and 2.89 eV [29]. For the $a^4\Sigma^-_{1/2}$, $a^4\Sigma^-_{3/2}$, $A^2\Delta_{3/2}$, and $A^2\Delta_{5/2}$ states, the SO coupling effect modifies the $T_e$, $\omega_e$, $\omega_e x_e$, and $\alpha_e$ by 419–641, 72.28–143.13, and 12.9276–37.7479, 0.0690–0.2506 $cm^{-1}$ relative to those obtained from MRCI+Q level. However, the SO coupling effect does not significantly modify the $B_e$ and $R_e$ values of the four Ω states. The SO splitting of $a^4\Sigma^-$ is calculated to be 38 $cm^{-1}$, which is consistent with previous experimental result of 26.08 $cm^{-1}$ [44]. It can be seen that $a^4\Sigma-$ 1/2 and $a^4\Sigma-$ 3/2 states have almost the same $R_e$, while the difference in $\omega_e$ and $\omega_e x_e$ values of the two Ω states are 213 $cm^{-1}$ and 31 $cm^{-1}$, which may arise from the strong SO coupling between $a^4\Sigma^-$–other low-lying excited states (the order of 100 $cm^{-1}$) and the relatively small $D_e$ (1.00 eV) of $a^4\Sigma^-$. The SO splitting of $A^2\Delta$ is calculated to be 194 $cm^{-1}$, which is evidently larger than previous experimental result of 20.6 $cm^{-1}$ [44] and theoretical value of 44.15 $cm^{-1}$ [52]. When only taking into account the SO coupling of the two lowest dissociation limits ($Ge(^3P_g)+H(^2S_g)$ and $Ge(^1D_g)+H(^2S_g)$), the calculated SO splitting of $A^2\Delta$ is reduced to 94 $cm^{-1}$, indicating that the SO splitting of the state is sensitive to the number of states included in the SO coupling calculation. Due to good agreement between our calculated data and the latest experimental results (Refs. [22,24,42]), we believe that our calculated SO splitting of $A^2\Delta$ (194 $cm^{-1}$) is more reliable.

With the aid of Λ–S compositions of the low-lying Ω states at several selected internuclear distances, the avoided crossing phenomenon between the states of the radical will be analyzed in detail. Fig. 4 shows that the shape of $A^2\Delta_{3/2}$ ((3)3/2) and $A^2\Delta_{5/2}$ ((1)5/2) Ω states obviously changes, as compared to that of $A^2\Delta$ Λ–S state. As shown in Fig. 1, the $A^2\Delta$ state crosses with $1^4\Pi$ state at $R$=2.45 Å. Taking into account the SO coupling effect, $A^2\Delta$ and $1^4\Pi$ states split into $A^2\Delta_{3/2}$, $A^2\Delta_{5/2}$, $1^4\Pi_{3/2}$, and $1^4\Pi_{5/2}$. Hence, the four Ω states will form an avoided crossing point near $R$=2.45 Å. The $2^2\Sigma^+$ state crosses with two repulsive states $1^4\Pi$ and $2^2\Pi$ around the internuclear distances of 2.0 and 2.25 Å, respectively. Since all the three Λ–S states have $\Omega$=1/2 component, there are two avoided crossing points around $R$=2.0 and R=2.25 Å. The crossing points between the $3^2\Sigma^+$ state and the two repulsive states $1^4\Pi$ and $2^2\Pi$ are located near $R$=1.80 Å and $R$=1.90 Å. Similarly, there are two avoided crossing points around $R$=1.80 Å and $R$=1.90 Å. As shown in Table 6, the dominant Λ–S compositions of both $A^2\Delta_{3/2}$ and $A^2\Delta_{5/2}$ states change from $^2\Delta$ (≈99%) at $R$=2.05 Å to $1^4\Pi$ (≈96%) at $R$=2.5 Å, that of (5)1/2($2^2\Sigma+$ 1/2) state

**Table 6**
Compositions of Ω states of GeH at selected internuclear distances.

| State | $r$ (Å) | $^2\Sigma^-$ | $1^2\Sigma^+$ | $2^2\Sigma^+$ | $3^2\Sigma^+$ | $4^2\Sigma^+$ | $1^2\Pi$ | $2^2\Pi$ | $3^2\Pi$ | $^2\Delta$ | $^4\Sigma^-$ | $^4\Sigma^+$ | $^4\Pi$ | $^4\Delta$ |
|---|---|---|---|---|---|---|---|---|---|---|---|---|---|---|
| $X^3\Pi_{1/2}$ | 1.6 | | | | | | 99.9 | | | | | | | |
| | 2.0 | | | | | | 99.9 | | | | | | | |
| | 2.05 | | | | | | 99.9 | | | | | | | |
| | 2.5 | | | | | | 99.7 | | | | | | | |
| $X^3\Pi_{3/2}$ | 1.6 | | | | | | 99.9 | | | | | | | |
| | 2.0 | | | | | | 99.9 | | | | | | | |
| | 2.05 | | | | | | 99.9 | | | | | | | |
| | 2.5 | | | | | | 99.7 | | | | | | | |
| (3)3/2 | 1.6 | | | | | | | | | 100 | | | | |
| ($A^2\Delta_{3/2}$) | 2.0 | | | | | | | | | 99.4 | | | | |
| | 2.05 | | | | | | | | | 99.4 | | | | |
| | 2.5 | | | | | | | | | 2.1 | | | 96.1 | |
| (1)5/2 | 1.6 | | | | | | | | | 99.4 | | | | |
| ($A^2\Delta_{5/2}$) | 2.0 | | | | | | | | | 99.2 | | | | |
| | 2.05 | | | | | | | | | 98.8 | | | | |
| | 2.5 | | | | | | | | | 1.0 | | | 97.3 | |
| (4)1/2 | 1.6 | | 99.1 | | | | | | | | | | | |
| | 1.85 | | 99.4 | | | | | | | | | | | |
| | 2.05 | | 99.3 | | | | | | | | | | | |
| | 2.3 | | 79.8 | | | | | | | | | | 19.7 | |
| (5)1/2 | 1.6 | | | 99.8 | | | | | | | | | | |
| | 1.85 | | | 98.0 | | | | | | | | | 1.7 | |
| | 2.05 | | | 20.2 | | | | | | | | | 79.2 | |
| | 2.30 | | 15.9 | 1.0 | | | | | | | | | 82.7 | |
| (6)1/2 | 1.6 | | | | 99.3 | | | | | | | | | |
| | 1.85 | | | 1.1 | 1.0 | | | | | | | | 96.7 | |
| | 2.50 | | 96.7 | | | | | | | | | | 2.4 | |
| (7)1/2 | 1.6 | | | | | | | | | | | | 99.6 | |
| | 2.05 | | | 77.4 | | | | | | | | | 22.2 | |
| | 2.30 | | | 5.7 | | | | 93.2 | | | | | | |
| (8)1/2 | 1.6 | | | | | | | | | | | | 99.1 | |
| | 1.85 | | | | 99.0 | | | | | | | | | |
| | 2.05 | | | | | | | 99.4 | | | | | | |
| | 2.3 | | | 92.8 | | | | 5.8 | | | | | | |
| (9)1/2 | 1.6 | | | | | | | 98.4 | | | | | | |
| | 1.85 | | | | | | | 99.5 | | | | | | |
| | 2.05 | | | | 99.7 | | | | | | | | | |
| | 2.3 | | | | 99.3 | | | | | | | | | |

changes from $2^2\Sigma^+$ (98.0%) at $R=1.85$ Å to $1^4\Pi$(79.2%) at $R=2.05$ Å, and that of (6)1/2($3^2\Sigma+$ 1/2) state changes from $3^2\Sigma^+$ (99.3%) at $R=1.6$ Å to $1^4\Pi$(96.7%) at $R=1.85$ Å. Owing to the avoided crossing with higher $\Omega=3/2$ and 5/2 states, both $A^2\Delta_{3/2}$ and $A^2\Delta_{5/2}$ states become quasibound and form potential maxima located at $R=2.45$ Å. The heights for the potential barrier of $A^2\Delta_{3/2}$ and $A^2\Delta_{5/2}$ states are 2695 $cm^{-1}$ and 2725 $cm^{-1}$, respectively, which can both hold two vibrational levels in their respective potential wells. The higher states (5)1/2 and (6)1/2 are found to be quasibound, and become repulsive at $R>2.05$ Å and $R>1.85$ Å, respectively.

### 3.4. Predissociation phenomenon and lifetimes of several electronic sates of GeH

The avoided crossing phenomenon discussed in Section 3.3 may lead to various possible predissociation pathways. The existence of SO-induced predissociation pathways is well described by spin–orbit matrix elements between two interacting Λ–S states in the crossing regions. Evolution of the absolute values of the correlated spin–orbit matrix elements along the internuclear distance is plotted in Fig. 5. For the $A^2\Delta$ and $1^4\Pi$ states, the crossing point ($R=2.45$ Å) is located between $\nu'=2$ and $\nu'=3$ vibrational levels of the $A^2\Delta$ state. At the crossing point, the absolute value of the SO matrix element is 315 $cm^{-1}$, which is high enough to induce such kind of SO predissociation for $A^2\Delta$ ($\nu'>2$) vibrational levels via the $1^4\Pi$ state. The predissociation for the $A^2\Delta$ state has been verified in experimental measurements [23,24], in which only the $\nu'=0$–2 vibrational levels of $A^2\Delta$ state were observed. For the $2^2\Sigma^+$ state, the two crossing points are located close to the classical turning points of $\nu'=0$ and $\nu'=1$ vibrational levels. At the two crossing points, the absolute value of the matrix elements of $2^2\Sigma^+$–$1^4\Pi$ and $2^2\Sigma^+$–$2^2\Pi$ are 468 and 165 $cm^{-1}$, respectively, which can cause the SO predissociation for $2^2\Sigma^+$ ($\nu'\geq 0$) vibrational levels via

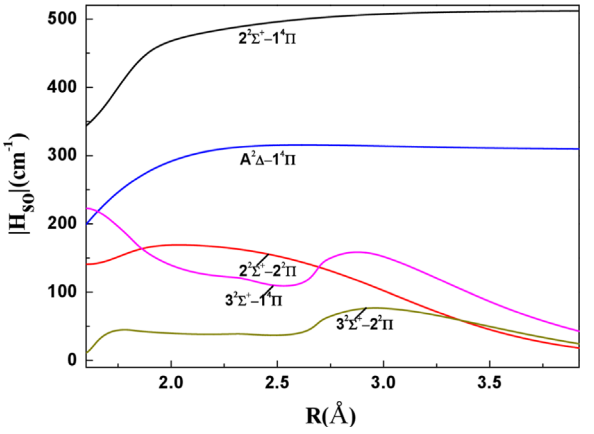


**Fig. 5.** Evolution of absolute value of spin–orbit matrix elements related to several Λ–S states versus internuclear distance.

the $1^4\Pi$ and $2^2\Pi$ states. Similarly, for the $3^2\Sigma^+$ state, two predissociation channels via $1^4\Pi$ and $2^2\Pi$ states are possible. At the crossing points, the maximum SO matrix elements of $3^2\Sigma^+$ ($180\ cm^{-1}$) are evidently smaller than that of $2^2\Sigma^+$ ($468\ cm^{-1}$), so the predissociation of $2^2\Sigma^+$ is more difficult to be detected, as compared to the $3^2\Sigma^+$ state. Thus, in combination with good agreement of $T_e$ value between our calculated one for $3^2\Sigma^+$ state and experimental one for $B^2\Sigma^+$, the $B^2\Sigma^+$–$X^2\Pi$ transition observed in experiment [17] can be safely assigned to the $3^2\Sigma^+$–$X^2\Pi$ transition.

The radiative lifetime of the vibrational level $\nu'$ for a given state is defined as the inverse of the total transition probability

$$\tau = \left(\sum_{\nu''} A_{\nu'\nu''}\right)^{-1} \tag{2}$$

The Einstein coefficient $A_{\nu'\nu''}$ between vibrational levels $\nu'$ and $\nu''$ is determined by

$$A_{\nu'\nu''} = 2.026 \times 10^{-6}\tilde{\upsilon}^3(\mathrm{TDM})^2 q_{\nu'\nu''} \tag{3}$$

where $\tilde{\upsilon}$ (in unit of $cm^{-1}$) is the energy difference between vibrational levels $\nu'$ and $\nu''$, TDM (in atomic unit) is the average electronic transition dipole moment in the region of classical turning point, $q_{\nu'\nu''}$ is the FCF of the two vibrational levels $\nu'$ and $\nu''$, and the radiative lifetime $\tau$ is in units of second.

Based on the computed TDMs, vibrational energy levels, and PECs, we calculated the radiative lifetimes of $a^4\Sigma-$ 1/2, $a^4\Sigma-$ 3/2, (2)3/2, and (1)5/2 states, which are listed in Table 7. Since the ground state is composed of doublet states $X^2\Pi_{1/2}$ ($X_1$) and $X^2\Pi_{3/2}(X_2)$, the radiative lifetime of the $\nu'$ level of a given state (such as $A^2\Delta_{3/2}$) is expressed as

$$\frac{1}{\tau_A^{rad,\nu'}} = \frac{1}{\tau_{A-X_1}^{rad,\nu'}} + \frac{1}{\tau_{A-X_2}^{rad,\nu'}} \tag{4}$$

The radiative lifetimes of $A^2\Delta_{3/2}$ and $A^2\Delta_{5/2}$ are calculated to be on the order of 100 ns, whereas those of $a^4\Sigma-$ 3/2 and $a^4\Sigma-$ 1/2 are computed to be on the order of 1 ms and 10 ms, by employing formula (4), respectively.

**Table 7**
Radiative lifetimes (in ns) of the low-lying vibrational levels of $A^2\Delta_i$ and $a^4\Sigma_i^-$.

| Transition | Partial radiative lifetimes of upper state | | Total radiative lifetimes of upper state | |
|---|---|---|---|---|
| | $\nu'=0$ | $\nu'=1$ | $\nu'=0$ | $\nu'=1$ |
| $A^2\Delta_{3/2}$–$X^2\Pi_{1/2}$ | 194 | 224 | 102 | 118 |
| $A^2\Delta_{3/2}$–$X^2\Pi_{3/2}$ | 215 | 250 | | |
| $A^2\Delta_{5/2}$–$X^2\Pi_{1/2}$ | 189 | 220 | 99 | 116 |
| $A^2\Delta_{5/2}$–$X^2\Pi_{3/2}$ | 210 | 245 | | |
| $a^4\Sigma_{1/2}$–$X^2\Pi_{1/2}$ | $3\times10^5$ | $3\times10^5$ | $2\times10^5$ | $2\times10^5$ |
| $a^4\Sigma_{1/2}$–$X^2\Pi_{3/2}$ | $4\times10^5$ | $4\times10^5$ | | |
| $a^4\Sigma_{3/2}$–$X^2\Pi_{1/2}$ | $2\times10^8$ | $3\times10^8$ | $1\times10^7$ | $6\times10^6$ |
| $a^4\Sigma_{3/2}$–$X^2\Pi_{3/2}$ | $1\times10^7$ | $6\times10^6$ | | |

For the $A^2\Delta_{3/2}$ state, our calculated total radiative lifetime of the $\nu'=0$ level is 102 ns, which is well consistent with previous theoretical result (130 ns) [23]. Our computed radiative lifetime of the state is also in good agreement with previous experimental value of $93\pm10$ ns [25], and conflicts with the experimental value of $12\pm2$ ns [24].

## 4. Conclusions

In conclusion, we have carried out comprehensive theoretical investigations of low-lying electronic states of GeH by employing the MRCI+Q method with large aug-cc-pwCV5Z-DK and aug-cc-pV5Z-DK basis sets for Ge and H, respectively. The scalar relativistic correction was determined by the third-order Douglas–Kroll and Hess one-electron integrals. The SO coupling effect was also taken into account via the state interaction method with the full Breit–Pauli Hamiltonian.

The PECs of eight Λ–S valence states, four low-lying Rydberg states, and those of 24 Ω states generated from the Λ–S states were computed. The spectroscopic parameters of $X^2\Pi$, $a^4\Sigma^-$ and $A^2\Delta$ states agree well with previous experimental results. Our calculated adiabatic transitional energy of $3^2\Sigma^+$ state (41,264 $cm^{-1}$ or 5.12 eV ) is in good accordance with that of the $B^2\Sigma^+$ state (41,074 $cm^{-1}$ or 5.09 eV) tentatively assigned in experiment. Thus, the observed $B^2\Sigma^+$ state is assigned to the $3^2\Sigma^+$ state correlated to the Rydberg asymptote (Ge($4s^24p5s$, $^3P_u$)+H($1s,^2S_g$)). With the aid of dominant Λ–S state compositional variation of Ω states at different internuclear distances, the avoided crossing phenomena of $A^2\Delta_{3/2}$, $A^2\Delta_{5/2}$, (5)1/2, and (6)1/2 states were analyzed in detail. For $A^2\Delta$ state, the crossing point lies between $\nu'=2$ and $\nu'=3$ vibrational levels, and the absolute value of $A^2\Delta$–$1^4\Pi$ spin–orbit matrix element is 315 $cm^{-1}$ around the crossing point, which can open predissociation channels $A^2\Delta$ ($\nu'>2$)→$1^4\Pi$. Near the crossing points, the maximum absolute value of SO matrix elements including $2^2\Sigma^+$ and $3^2\Sigma^+$ are 468 and 180 $cm^{-1}$, respectively, which could lead to the predissociation for the $\nu'>0$ vibrational levels of $2^2\Sigma^+$ and $3^2\Sigma^+$ states. The TDMs of the bound Ω states to the ground state $X^2\Pi$ were

investigated, and the radiative lifetimes of several low-lying vibrational levels of $a^4\Sigma^-_{1/2}$, $a^4\Sigma^-_{3/2}$, $A^2\Delta_{3/2}$ and $A^2\Delta_{5/2}$ states were evaluated. It is expected that our theoretical study provides more helpful information for further investigations on electronic structures and spectroscopic properties of the GeH radical.

## Acknowledgments

This work was supported by the National Natural Science Foundation of China (11074095, 11274140, and 11404180) and the Natural Science Foundation of Heilongjiang Province (F201335). We acknowledge the High Performance Computing Center (HPCC) of Jilin University for supercomputer time.

## Appendix A. Supporting information

Supplementary data associated with this article can be found in the online version at http://dx.doi.org/10.1016/j.jqsrt.2015.02.009.

## References

[1] Andreatta RW. Low-temperature growth of polycrystalline Si and Ge films by ultraviolet laser photodissociation of silane and germane. Appl Phys Lett 1982;40:183–5.
[2] Osmundsen JF, Abele CC, Eden JG. Activation energy and spectroscopy of the growth of germanium films by ultraviolet laser-assisted chemical vapor deposition. J Appl Phys 1985;57:2921–30.
[3] Li QS, Lü RH, Xie Y, Schaefer HF. Molecules for materials: Germanium hydride neutrals and anions. molecular structures, electron affinities, and thermochemistry of $GeH_n$/GeH–n ($n$=0–4) and $Ge_2H_n$/$Ge_2H$–$n$ ($n$=0–6). J Comput Chem 2002;23:1642–55.
[4] Binning RC, Curtiss LA. Theoretical study of $GeH_n$, $AsH_n$, and $SeH_n$: ionization energies. J Chem Phys 1990;92:3688–92.
[5] Ruscic B, Schwarz M, Berkowitz J. Photoionization studies of $GeH_n$ ($n$=2–4). J Chem Phys 1990;92:1865–75.
[6] Operti L, Rabezzana R, Turco F, Vaglio GA. Negative gas-phase ion chemistry of $GeH_4$: a quadrupole ion trap study. Rapid Commun Mass Spectrom 2005;19:1963–9.
[7] Antoniotti P, Rabezzana R, Turco F, Borocci S, Giordani M, Grandinetti F. Ion chemistry in germane/fluorocompounds gaseous mixtures: a mass spectrometric and theoretical study. J Mass Spectrom 2008;43:1320–33.
[8] Hoshino M, Matejčík Š, Nunes Y, Ferreira da Silva F, Limão-Vieira P, Tanaka H. Negative ion formation through dissociative electron attachment to $GeH_4$: comparative studies with $CH_4$ and $SiH_4$. Int J Mass Spectrom 2011;306:51–6.
[9] Antoniotti P, Operti L, Rabezzana R, Turco F, Zanzottera C, Giordani M, et al. Gas-phase reactions of XH+3 ($X$=C, Si, Ge) with $NF_3$: a comparative investigation on the detailed mechanistic aspects. J Mass Spectrom 2009;44:1348–58.
[10] Mineva T, Russo N, Sicilia E, Toscano M. Spectroscopic constants of $SiH_2$,$GeH_2$, $SnH_2$, and their cations and anions from density functional computations. Int J Quantum Chem 1995;56:669–75.
[11] Smith TC, Clouthier DJ, Sha W, Adam AG. Laser optogalvanic and jet spectroscopy of germylene ($GeH_2$): new spectroscopic data for an important semiconductor growth intermediate. J Chem Phys 2000;113:9567–76.
[12] Lemierre V, Chrostowska A, Dargelos A, Baylère P, Leigh WJ, Harrington CR. Flash vacuum thermolysis of 3,4-dimethyl-1-germacyclopent-3-enes: UV photoelectron spectroscopic characterization of $GeH_2$ and $GeMe_2$. Appl Organomet Chem 2004;18:676–83.
[13] Tokue I, Ebina S, Kanai M, Nanbu S. The vibrational structure of the $\tilde{X}\ ^1A_1-\tilde{A}\ ^1B_1$ and $\tilde{A}\ ^1B_1-\tilde{B}\ ^1A_1$ band systems of $GeH_2$/$GeD_2$ based on global potential energy surfaces. J Chem Phys 2007;126:044313.
[14] Matsunaga N, Koseki S, Gordon MS. Relativistic potential energy surfaces of XH ($X$=C, Si, Ge, Sn, and Pb) molecules: coupling of A and B states. J Chem Phys 1996;104:7988–96.
[15] Kleman B, Werhagen E. $A^2\Delta$–$^2\Pi$ system in germanium hydride (GeH). Ark Fys 1953;6:359.
[16] Kleman B, Werhagen E. $A^4\Sigma^-$–$^2\Pi$ system in germanium hydride (GeH). Ark Fys 1953;6:399.
[17] Barrow RF, Drummond G, Garton WRS. Ultra-violet bands associated with germanium. Proc Phys Soc Sect A 1953;66:191–2.
[18] Klynning L, Lindgren B. Rotational analysis of the $^2\Delta$–$^2\Pi$ band system of germanium hydride and of deuteride germanium. Ark Fys 1966;32:575.
[19] Towle JP, Brown JM. The infrared spectrum of the GeH radical by laser magnetic resonance. Mol Phys 1990;70:161–5.
[20] Petri M, Simon U, Zimmermann W, Urban W, Towle JP, Brown JM. Infrared diode laser spectroscopy of the ground state of GeH ($X^2\Pi_{1/2}$). Mol Phys 1991;72:315–9.
[21] Akiyama Y, Tanaka K, Tanaka T. Infrared diode laser spectroscopy of the GeH radical in the $^2\Pi_{1/2}$ state. J Chem Phys 1991;94:3280–1.
[22] Towle JP, Brown JM. The infrared spectrum of the GeH radical. Mol Phys 1993;78:249–61.
[23] Erman P, Gustafsson O, Larsson M. New predissociations in GeH affecting all the $A^2\Delta$ state levels. Phys Scr 1983;27:256–60.
[24] Osmundsen JF, Abele CC, Eden JG. Multiphoton dissociation of $GeH_4$: ultraviolet emission spectrum of GeH. J Chem Phys 1985;83:2159–61.
[25] Bauer W, Engelhardt B, Wiesen P, Becker KH. Lifetime measurements of GeH and CH in the $A^2\Delta$, $v'=0$ state by laser-induced fluorescence. Chem Phys Lett 1989;158:321–4.
[26] Balasubramanian K, Li J. Spectroscopic properties and potential energy surfaces of GeH. J Mol Spectrosc 1988;128:413–26.
[27] Bruna PJ, Grein F. Ab Initio study of the $X^3\Sigma^-$, $a^1\Delta$, $b^1\Sigma^+$ states of $GeH^-$, and electron affinity of GeH. J Mol Struct 2001;599:261–9.
[28] Song C, Gao T, Han H, Wan M, Yu Y. Ab initio study of spin–orbit interaction in the ground electronic states of XH (X=C, Si, Ge and Sn) molecules. J Mol Struct THEOCHEM 2008;870:65–71.
[29] Li H, Feng H, Sun W, Xie Y, Schaefer HF. Diatomic silylynes, germylynes, stannylynes, and plumbylynes: structures, dipole moments, dissociation energies, and quartet–doublet gaps of EH and EX (E=Si, Ge, Sn, Pb; X=F, Cl, Br, I). Inorg Chem 2013;52:6849–59.
[30] Minaev BF, Knuts S, Ågren H. On the interpretation of the external heavy atom effect on singlet–triplet transitions. Chem Phys 1994;181:15–28.
[31] Deonker NJ, Allen WD. Taming the low-lying electronic states of FeH. J Chem Phys 2012;137:234303.
[32] Werner H-J, Knowles PJ, Lindh R, Manby FR, Schütz M, Celani P, et al. MOLPRO, a package of ab initio programs; 2010 ⟨http://www.molpro.net⟩.
[33] Werner H-J, Knowles PJ. A second order multiconfiguration SCF procedure with optimum convergence. J Chem Phys 1985;82:5053–63.
[34] Werner H-J, Knowles PJ. An efficient internally contracted multiconfiguration-reference configuration interaction method. J Chem Phys 1988;89:5803–14.
[35] Langhoff SR, Davidson ER. Configuration interaction calculations on the nitrogen molecule. Int J Quantum Chem 1974;8:61–72.
[36] Douglas M, Kroll NM. Quantum electrodynamical corrections to the fine structure of helium. Ann Phys 1974;82:89–155.
[37] Hess BA. Relativistic electronic-structure calculations employing a two-component no-pair formalism with external-field projection operators. Phys Rev A 1986;33:3742–8.
[38] LeRoy RJ. LEVEL7.7: a computer program for solving the radial Schrödinger equation for bound and quasibound levels.Chemical Physics Research Report CP-661. Ontario, Canada: University of Waterloo; 2005.
[39] Wilson AK, Woon DE, Peterson KA, Dunning TH. Gaussian basis sets for use in correlated molecular calculations. IX. The atoms gallium through krypton. J Chem Phys 1999;110:7667–76.
[40] DeJong WA, Harrison RJ, Dixon DA. Parallel Douglas–Kroll energy and gradients in NWChem: estimating scalar relativistic effects using Douglas–Kroll contracted basis sets. J Chem Phys 2001;114:48–53.
[41] DeYonker NJ, Peterson KA, Wilson AK. Systematically convergent correlation consistent basis sets for molecular core−valence correlation effects: the third-row atoms gallium through krypton. J Phys Chem A 2007;111:11383–93.
[42] Moore CE. Atomic energy levels. Washington, DC: National Bureau of Standard; 1971.
[43] Dunning TH. Gaussian basis sets for use in correlated molecular calculations. I. The atoms boron through neon and hydrogen. J Chem Phys 1989;90:1007–23.

[44] Huber KP, Herzberg G. Molecular spectra and molecular structure IV, constants of diatomic molecules. New York: Van Nostrand Reinhold; 1979.
[45] Kalemos A, Mavridis A, Metropoulos A. An accurate description of the ground and excited states of CH. J Chem Phys 1999;111:9536–48.
[46] Kalemos A, Mavridis A, Metropoulos A. An accurate description of the ground and excited states of SiH. J Chem Phys 2002;116:6529–40.
[47] Werner H-J, Buckingham AD. An accurate ab initio calculation of the dipole moment function of GeH. Chem Phys Lett 1986;125:433–7.
[48] Pettersson LGM, Langhoff SR. Theoretical electric dipole moments of SiH, GeH and SnH. Chem Phys Lett 1986;125:429–32.
[49] Chapman DA, Li J, Balasubramanian K, Lin SH. Theoretical study of electric dipole and transition moments of GeH, SnH, and PbH. J Chem Phys 1988;88:3826–33.
[50] Brown JM, Evenson KM, Sears TJ. Infrared and far-infrared laser magnetic resonance spectroscopy of the GeH radical: determination of ground state parameters. J Chem Phys 1985;83:3275–84.
[51] Ashworth SH, Brown JM. The electric dipole moments of SeH and GeH in their ground $^2\Pi$ states. Chem Phys Lett 1991;182:73–80.
[52] Chang YW, Sun H. Spin–orbit splittings in the valence states of XH (X=K, Ca, Ga, Ge, As, Se, and Br) by the effective Hamiltonian approach. Chem Phys Lett 2010;493:371–5.
[53] Veseth L. Some anomalies in the electronic spectra of GeH, GeD, SnH, and SnD related to Hund's coupling case (c). J Mol Spectrosc 1973;48:283–91.
[54] Veseth L. Second-order spin–orbit splitting in $^2\Delta$ states of diatomic molecules. Physica 1971;56:286–93.